ISSN 1070-3632, Russian Journal of General Chemistry, 2014, Vol. 84, No. 5, pp. 927–933. © Pleiades Publishing, Ltd., 2014.
Original Russian Text © E.A. Katlenok, K.P. Balashev, 2014, published in Zhurnal Obshchei Khimii, 2014, Vol. 84, No. 5, pp. 835–842.

Complexes of Rh(III), Ir(III), and Pt(IV) with Metallated 2-(*n*-Tolyl)pyridine, Ethylendiamine, Acetate, and Diethyldithiocarbamate Ligands

E. A. Katlenok and K. P. Balashev

Herzen State Pedagogical University of Russia, nab. r. Moiki 48, St. Petersburg, 191186 Russia
e-mail: balashevk@mail.ru

Received February 11, 2014

Abstract—*cis*-C,C Isomers of the $[M(ptpy)_2(L\hat{}L)](PF_6)_Z$ complexes [M = Rh(III), Ir(III), Pt(IV); $ptpy^-$ = deprotonated form of 2-(*n*-tolyl)pyridine, (L^L) = acetate, trifluoroacetate, or diethyldithiocarbamate anions, or ethylenediamine; *z* = 0, 1, 2] were prepared and characterized by ^1H and ^{19}F NMR, IR, electronic absorption and emissions spectroscopy, and by voltammetry methods. The highest occupied and the lowest unoccupied molecular orbitals were assigned to d_π and π^*_{ptpy} orbitals of the metal and the metallated ligand. Luminescence of the complexes in the visible spectral region was assigned to the spin-forbidden optical transition from the lowest energy state of the mixed nature (π_{ptpy}–π^*_{ptpy}/d_x–π^*_{ptpy}).

Keywords: cyclometallated complex, electron-excited states

DOI: 10.1134/S1070363214050247

Electronic structure of photoexcited cyclometallated complexes of platinum-metals is characterized by strong phosphorescence in the visible spectral region; the one-electronic outer-sphere electron transfer processes are typical of such compounds. These properties provide for wide possibilities of their application as activators of organic light-emitting diodes [1–3], luminescent sensors [4, 5], and biological labels [6]. The data collected on behavior of Pt(II) and Ir(III) mixed-ligand complexes demonstrates that optical and electrochemical properties of the complexes can be changed by varying the ligands nature. Octahedral complexes of Rh(III) and Pt(IV) have been much less studied; that limits the range of their optical and electrochemical properties to be achieved purposefully.

Herein, we report on the influence of the metal nature and of donor-acceptor properties of the chelating ligands on optical and electrochemical properties of the $[M(ptpy)_2(L\hat{}L)]^z$ complexes [M = Rh(III), Ir(III), Pt(IV); $ptpy^-$ = deprotonated form of 2-(*n*-tolyl)pyridine, (L^L) = ethylenediamine (En), acetate (OAc^-), trifluoroacetate(OTf^-), and diethyldithiocarbamate (dtc^-)] (Scheme 1).

Scheme 1.

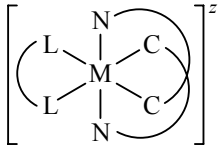

M = Pt(IV), Ir (III), Rh(III)

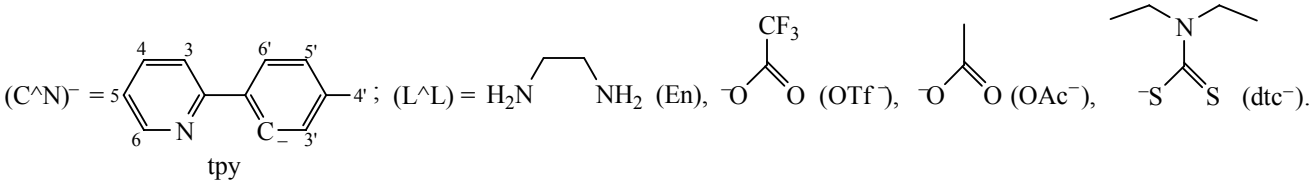

Table 1. Chemical shifts (δ, ppm) and spin-spin coupling constants ($^3J_{HPt}$, Hz) in ^1H and ^{19}F MNR spectra of the $[M(ptpy)(L^{\wedge}L)]^z$ complexes

Complex	{M(ptpy)}								{M(L^L)}
	H^3	H^4	H^5	H^6	$H^{3'}$	$H^{4'}$	$H^{5'}$	$H^{6'}$	
$[Rh(ptpy)_2dtc]$[a]	7.80	7.79	7.19	9.52	6.13	2.02	6.67	7.50	3.94, 3.67 (CH_2) 1.21, 1.21 (CH_3)
$[Ir(ptpy)_2dtc]$[a]	7.82	7.71	7.16	9.59	6.15	2.04	6.61	7.47	3.79,3.52 (CH_2) 1.23, 1.23 (CH_3)
$[Pt(ptpy)_2dtc]PF_6$[a]	8.23	7.67	7.53	9.53 (25)	5.87	2.10	6.94	7.58	3.71, 3.60 (CH_2) 1.20, 1.22 (CH_3)
$[Rh(ptpy)_2OAc]$[a]	7.81	7.88	7.25	8.84	5.95	2.01	6.69	7.46	2.02 (CH_3)
$[Ir(ptpy)_2OAc]$[a]	7.83	7.77	7.23	8.82	5.88	2.00	6.60	7.40	2.02 (CH_3)
$[Pt(ptpy)_2OAc]PF_6$[b]	8.39	8.38	7.75	9.67 (27)	5.69 (33)	2.04	6.97	7.82	2.07 (CH_3)
$[Rh(ptpy)_2OTf]$[a]	7.82	7.88	7.25	8.82	5.98	2.03	6.73	7.46	–75.40 (CF_3)
$[Ir(ptpy)_2OTf]$[a]	7.80	7.79	7.23	8.83	5.93	2.04	6.65	7.40	–75.27 (CF_3)
$[Pt(ptpy)_2OTf]PF_6$[a]	7.92	8.12	7.53	9.42 (26)	5.68 (34)	2.10	6.95	7.45	–75.14 (CF_3)
$[Rh(ptpy)_2En]PF_6$[b]	8.16	8.07	7.47	8.75	5.91	1.95	6.70	7.70	4.18, 3.41 (NH_2) 2.78, 2.51 (CH_2)
$[Ir(ptpy)_2En]PF_6$[b]	8.13	7.98	7.41	8.81	5.96	1.96	6.63	7.63	4.88, 3.94 (NH_2) 2.74, 2.45 (CH_2)
$[Pt(ptpy)_2En](PF_6)_2$[b]	8.41	7.98	7.45	8.83 (32)	5.76 (21)	2.09	7.13	7.85	6.09, 5.58 (NH_2) 3.12, 2.82 (CH_2)

[a] $CDCl_3$. [b] $(CD_3)_2SO$.

^1H and ^{19}F MNR data (Table 1) pointed at the presence of two magnetically equivalent metallated ptpy ligands and one chelating L^L ligand in the inner sphere. Considerable upfield shifts of the $H^{3'–6'}$ signals of the metallated tolyl fragment $[M(ptpy)_2]$, Δδ –(0.3–1.6) ppm as compared to free 2-(*n*-tolyl)pyridine revealed anisotropic interaction of their circular currents in *cis*-C,C-complexes $[M(ptpy)_2(L^{\wedge}L)]^z$. In contrast to $H^{3'–6'}$ signals shifted upfield, the *trans*-positioning of pyridine fragments led to the downfield shift of the $H^{3–6}$ signals, Δδ +(0.2–0.9) ppm. Strengthening of the donor-acceptor ptpy → M interaction in the case of Pt(IV) as compared with Rh(III) and Ir(III) was reflected in more prominent downfield shift of the H^6 signal.

A special feature of the ^1H MNR spectra of coordinated chelating ligands $dtc^–$ and En is magnetic nonequivalence of protons in each pair or chemically identical groups (C_2H_5, CH_2, and NH_2, Table 1), revealing distortion of the octahedral structure of $[M\ ptpy)_2(L^{\wedge}L)]^z$ complexes. Donor-acceptor dtc → M interaction led to the upfield shift of the C_2H_5 proton signals, whereas the En → M interaction resulted in the downfield shift of the NH_2 and C_2H_5 proton signals.

The IR spectra of $[M(ptpy)_2(L^{\wedge}L)]^z$ complexes contained bands assigned to characteristic vibrations of the metallated and the chelating inner-sphere ligands along with those of outer-sphere $PF_6^–$ ion (Table 2). Coordination of 2-(*n*-tolyl)pyridine to metal ions via N and C donor atoms was accompanied by decrease in frequencies of C=C/C=N vibrations as well as by characteristic [7] change of C−H bending vibrations at 819 ± 6 and 875 ± 3 $cm^{–1}$.

In agreement with the ^1H MNR data (Table 1), strengthening of the En→M donor-acceptor interaction in the Rh(III) < Ir(III) < Pt(IV) series led to red shift of the NH_2 and CH_2 vibration bands of coordinated ethylenediamine (Table 2). The chelating type of

Table 2. Characteristic vibration frequencies (KBr, cm^{-1}) of the ligands coordinated in $[M(ptpy)(L\hat{}L)]^z$ complexes

Complex	{M(ptpy)}		{M(L^L)}		PF_6^-
	ν(C=C/C=N)	ν(C–H)			
$[Rh(ptpy)_2dtc]$	1600, 1585, 1481	827, 877	1477 (CN)	993 (CS)	–
$[Ir(ptpy)_2dtc]$	1603, 1588, 1489	812, 877	1473 (CN)	995 (CS)	–
$[Pt(ptpy)_2dtc]PF_6$	1610, 1591, 1490	[a]	1466[b] (CN)	995 (CS)	843
$[Rh(ptpy)_2OAc]$	1604, 1586, 1480	816, 870	1427[b], 1563 (COO)	–	–
$[Ir(ptpy)_2OAc]$	1605, 1589, 1477	817, 877	1428[b], 1561 (COO)	–	–
$[Pt(ptpy)_2OAc]PF_6$	1609, 1593, 1492	[a]	1433, 1566[b] (COO)		845
$[Rh(ptpy)_2OTf]$	1605, 1587, 1481	824, 875	1428[b], 1625 (COO)	–	–
$[Ir(ptpy)_2OTf]$	1605, 1589, 1479	815, 874	1428[b], 1618 (COO)	–	–
$[Pt(ptpy)_2OTf]PF_6$	1613[b], 1594, 1496	[a]	1435, 1613[b] (COO)	–	844
$[Rh(ptpy)_2En]PF_6$	1606, 1588, 1480	[a]	3316, 3360 (NH_2)	1597 (NH_2)	844
$[Ir(ptpy)_2En]PF_6$	1602, 1590, 1477	[a]	3308, 3350 (NH_2)	1601 (NH_2)	847
$[Pt(ptpy)_2En](PF_6)_2$	1612, 1593[b], 1494	[a]	3289, 3313 (NH_2)	1593[b] (NH_2)	843

[a] Overlapping with PF_6^- band. [b] Bands overlapping.

coordination in the cases of OAc^-, OTf^-, and dtc^- was confirmed by characteristic [7] difference of frequencies of the antisymmetric and symmetric COO^- vibrations in OAc^- (133 ± 3 cm^{-1}) and OTf^- (188 ± 10 cm^{-1}) ligands as well as by the absence of splitting of the C–S band at 994 ± 1 cm^{-1} [8].

In the frame of the model of predominant localization of molecular orbitals [9], optical and electrochemical processes involving complexes can be divided into metal-centered, ligand-centered, and metal-ligand charge transfer processes. In the electronic absorption spectra of the studied complexes (Table 3), two types of spin-allowed optical transitions were observed. In the short-wave region ($\lambda < 330$ nm), independently of the metal and the chelating ligand nature, strong ($\varepsilon \sim 10^4$ L mol^{-1} cm^{-1}) vibronic bands were observed, slightly differing on the position from the bands of free 2-(*n*-tolyl)pyridine [10]. They were assigned to intraligand (IL) π–π* optical transitions of the heterocyclic ligand $ptpy^-$ in $[M(ptpy)_2]$ fragments. In the longer-wave range, weaker ($\varepsilon \sim 10^3$ L mol^{-1} cm^{-1}) and broad absorption bands exhibited red shift both with increasing the energy of metal valent *d*-orbitals in the Pt(IV) < Rh(III) < Ir(III) series (Fig. 1) and upon ethylenediamine (σ-donor) was replaced by acetate or diethyldithiocarbamate chelating ligands (σ- and π-donors) (Fig. 2). Therefore, the long-wave absorption bands of $[M(ptpy)_2(L\hat{}L)]^z$ complexes could be assigned to the envelope of the vibronic band optical metal-ligand charge transfer transitions $d–\pi^*_{ptpy}$ (MLCT). Weak [ε (0.3–0.9) $\times 10^3$ L mol^{-1} cm^{-1}] absorption bands at 485 and 482 nm observed in the cases of $[Ir(ptpy)_2OTf]$ and $[Ir(ptpy)_2dtc]$ (Table 3) were apparently caused by spin-forbidden optical transitions of the mixed type (IL/MLCT).

Assuming that Koopmans' theorem [11] is held for the complexes under study, the highest occupied and the lowest unoccupied molecular orbitals participating in the spin-allowed optical transition and electrochemical oxidation and reduction of the complexes should be of the similar nature.

In agreement with the presence of two metallated heterocyclic ligands $ptpy^-$ in the inner sphere of Rh(III) and Ir(III) complexes $[M(ptpy)_2(L\hat{}L)]^z$, independently of the (L^L) chelating ligand nature, voltamperograms of their reduction were characterized by two irreversible single-electron waves with current peaks potentials of $–2.6 \pm 0.2$ and $–3.0 \pm 0.2$ V (Table 3). It pointed at the ligand-centered type of Rh(III) and Ir(III) complexes reduction as a result of consecutive

Table 3. Optical and electrochemical parameters of $[M(ptpy)(L^{\wedge}L)]^{z}$ complexes

Complex	Absorption (λ), nm ($\varepsilon \times 10^3$, L mol^{-1} cm^{-1})[a]	Emission (λ), nm (τ, μs)		Excitation (λ), nm (77 K)[c]	E^{Ox}, V[d]	E^{Red}, V[d]
		293 K[a]	77 K[c]			
[Rh(ptpy)$_2$dtc]	243 (51.7), 288 sh (34), 304 sh (26), 340 sh (7.9), 390 (5.73)	–	462, 494, 524, 564 (80)	312 sh, 330 sh, 344, 386	0.79	–2.76 –3.02
[Rh(ptpy)$_2$OTf]	249 (29.4), 270 sh (26), 307 sh (17), 390 (3.19), 404 sh (2.0)	–	466, 498, 534 sh (110)	310 sh, 325 sh, 364, 385	1.25	–2.50 <–3.0
[Rh(ptpy)$_2$OAc]	270 (26.6), 308 (16.8), 402 (4.91),	–	468, 502, 540 sh (110)	310 sh, 326 sh, 349, 386	0.75[д]	–2.48[e] –2.79[e]
[Rh(ptpy)$_2$En]PF$_6$	246 (21.5), 267 (21.6), 300 (12.8),	–	462, 482 sh, 496, 535 (110)	310 sh, 325 sh, 350, 385	0.83[b]	–2.47[b] –2.77[b]
[Ir(ptpy)$_2$dtc]	236 (40.2), 265 (35.9), 288 sh (33), 300 sh (30), 352 (8.12), 378 sh (6.3), 404 (4.83), 450 sh (2.4),	502, 546 sh (6)	486, 520, 563 sh, 602 sh (6)	313 sh, 347, 363, 378, 402, 424, 446, 479	0.54[f]	–3.04 –3.30
[Ir(ptpy)$_2$OTf]	263 (37.0), 276 sh (34), 308 sh (21), 356 sh (5.7), 403 (3.65), 434 (2.78), 458 sh (1.6), 485 (0.29)	514, 540 sh, 557 sh	491, 523, 564 sh (7)	312 sh, 331 sh, 349, 352, 362, 394, 425, 484	0.46[f]	–2.58 –3.06
[Ir(ptpy)$_2$OAc]	268 (41.9), 316 sh (19), 364 (6.80), 403 (4.50), 459 (3.85)	514, 557 sh,	493, 527, 572 sh (6)	310 sh, 331, 349, 376, 396, 425,	0.45[a,f]	–2.65[e] –2.81[e]
[Ir(ptpy)$_2$En]PF$_6$	262 (28.1), 275 sh (27), 317 sh (11), 352 sh (5.2), 432 sh (1.9)[b]	494, 513, 531 sh	485, 520, 564 sh, 603 sh (6)	310 sh, 325, 347, 361, 378 sh, 397, 425	0.55[b,f]	–2.61[b] –2.93[b]
[Pt(ptpy)$_2$dtc]PF$_6$	234 (47.6), 266 (41.0), 315 (20.1), 332 sh (16), 348 sh (11)	460, 489,	452, 485, 523 sh, 558 sh, 598 sh	300, 312, 329, 342	>2[b]	–1.94[b]
[Pt(ptpy)$_2$OTf]PF$_6$	264 (25.7), 274 sh (24), 312 sh (14), 330 (17.4), 340 sh (17)[b]	461, 491,	455, 488, 516 (290)	312, 328 sh, 338	>2[b]	–1.90[b]
[Pt(ptpy)$_2$OAc]PF$_6$	266 (30.2), 275 sh (29), 298 (12.6), 312 sh (17), 328 (19.8),	458, 489,	454, 487, 515, 554, 600 (320)	310, 329, 340	>2[b]	–1.69[b]
[Pt(ptpy)$_2$En](PF$_6$)$_2$	252 (45.2), 275 sh (31), 315 sh (20),	457, 489,	454, 476 sh, 488, 515, 554 (320)	311, 327, 341 sh	>2[b]	–1.47[b]

[a] CH_2Cl_2. [b] CH_3CN. [c] $CH_3OCH_2CH_2OH$–C_2H_5OH, 1 : 1. [d] Peak current potential at a scanning rate of 100 mV/s, $C_6H_5CH_3$–CH_3CN (1 : 1). [e] $(CH_3)_2NCOH$. [f] $E_{1/2}$.

transfer of two electrons onto the π*-orbitals of two metallated ptpy$^-$ ligands.

$$[M(ptpy)_2(L^{\wedge}L)]^{z} + e^- = [M(ptpy^-)(ptpy)(L^{\wedge}L)]^{z-1},$$

$$[M(ptpy^-)(ptpy)(L^{\wedge}L)]^{z-1} + e^- = [M(ptpy^-)_2(L^{\wedge}L)]^{z-2}.$$

The $[Pt(ptpy)_2(L^{\wedge}L)]^{z}$ complexes revealed the two-electron irreversible reduction wave shifted towards anode, with a peak current potential of –1.8 ± 0.2 V. It was assigned to the metal-centered reduction of platinum(IV) into platinum(II).

$$[Pt(ptpy)_2(L^{\wedge}L)]^{z} + 2e^- = \text{Pt(II) compound}.$$

Similarly, oxidation voltamperograms of Rh(III) and Ir(III) complexes contained single-electron irreversible [Rh(III)] and quasireversible [Ir(III)] waves, whereas oxidation of Pt(IV) complexes occurred outside the stability window of the solvent (>3 V). The

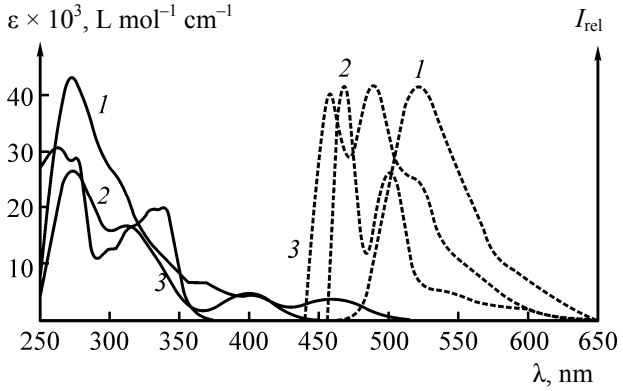

Fig. 1. Electronic absorption (solid lines) and emission (dashed lines) spectra of $[M(ptpy)_2(L\text{^}L)]^z$ complexes in various solvents. (*1*) $[Ir(ptpy)_2OAc]$ (293 K, CH_2Cl_2), (*2*) $[Rh(ptpy)_2OAc]$ (293 K, CH_2Cl_2 and 77 K, 2-metoxyethanol–ethanol, 1 : 1), (*3*) $[Pt(ptpy)_2OAc]PF_6$ (293 K, CH_3CN).

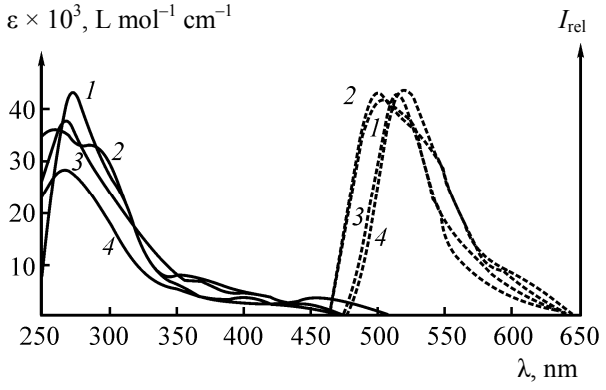

Fig. 2. Electronic absorption (solid lines) and emission (dashed lines) spectra of $[M(ptpy)_2(L\text{^}L)]^z$ complexes in various solvents. (*1*) $[Ir(ptpy)_2En]PF_6$ (CH_3CN), (*2*) $[Ir(ptpy)_2dtc]$ (CH_2Cl_2), (*3*) $[Ir(ptpy)_2OAcF]$ (CH_2Cl_2), (*4*) $[Ir(ptpy)_2OAc]$ (CH_2Cl_2).

increase of the complexes oxidation potential in the Pt(IV) < Rh(III) < Ir(III) series and the decrease of π-donating ability of the chelating (L^L) ligands (Table 2) was in agreement with the decrease of metal d_π-orbitals energy, reflecting the metal-centered nature of the electrochemical process.

$$[M^{III}(ptpy)_2(L\text{^}L)]^z - e^- = [M^{IV}(ptpy)_2(L\text{^}L)]^{z+1}.$$

Taking into account the assignment of long-wave absorption bands of Rh(III) and Ir(III) complexes to the d_π–π^*_{ptpy} MLCT optical transitions, the electrochemical data showed that LUMO and HOMO of the complexes were presumably localized at π* and d_π orbitals. Noteworthily, the energy of MLCT absorption bands was correlated with the oxidation potential of Rh(III) and Ir(III) complexes (Fig. 3). The metal-centered type of reduction and oxidation of Pt(IV) complexes suggested that the long-wave optical transition *d*–*d** ($\varepsilon \sim 10^2$ L mol^{-1} cm^{-1}) should have been observed [12]. However, the strong ($\varepsilon \sim 10^4$ L mol^{-1} cm^{-1}) MLCT bands (Table 3) could possibly mask *d*–*d**-bands in the absorption spectra of Pt(IV) complexes.

To summarize, the effect of nature of the metal [Pt(IV), Ir(III), Rh(III)] and the chelating ligand (L^L) in the $[M(ptpy)_2(L\text{^}L)]^z$ complexes on the position of spin-allowed bands in electronic absorption spectra and on their oxidation potentials was mainly due to changes of the complexes HOMO energy, that is, metal d_π-orbitals (Fig. 4).

In contrast to fluorescence of free 2-(*n*-tolyl)pyridine in UV region (λ_{max} 322 nm), photoexcitation of the complexes in the range of intraligand optical transitions and MLCT absorption bands (Figs. 1 and 2) led to phosphorescence in the visible (458−514 nm) range, with exponential decay kinetics (τ = 320−326 μs), which was due to the fact that the metal spin-orbital interaction (ξ = 1500−5000 cm^{-1} [13]) stimulated singlet-triplet interconversion of the excited states. Phosphorescence excitation spectra of the complexes were in agreement with their absorption spectra (Table 3).

Unlike Pt(IV) and Ir(III) complexes exhibiting phosphoresce at 293 and 77 K, the phosphorescence of Rh(III) complexes was only observed in the frozen (77 K) solutions. The thermal quenching of phosphorescence of Rh(III) complexes could arise from the less prominent splitting of *d*-orbitals, as compared with the Ir(III) and Pt(IV) complexes. Indeed, that should lead to the thermally activated population of metal-centered *d*–*d** excited states; the latter were subject to

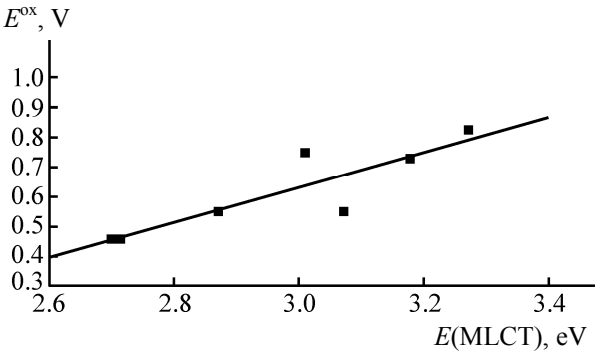

Fig. 3. Correlation of energies of MLCT absorption bands and oxidation potentials of Rh(III) and Ir(III) complexes.

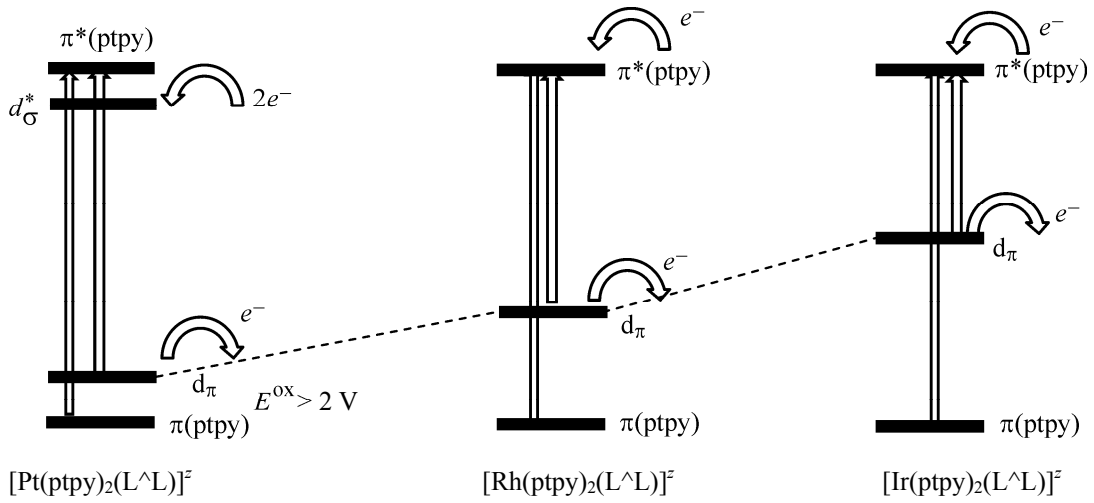

Fig. 4. Qualitative diagrams of molecular orbitals responsible for absorption spectra, oxidation and reduction of $[M(ptpy)_2(L\hat{}L)]^z$ complexes.

fast radiationless deactivation, being close in energy to the lowest excited intraligand state [14].

The energy positions of spin-forbidden intraligand, metal-ligand charge transfer, and *d–d** optical transitions were defined both by the energy position of the corresponding spin-allowed transitions and by the energy of their singlet-triplet splitting [15], which was of ~10^4 cm^{-1} in the case of intraligand transitions and was less than 5×10^3 cm^{-1} in the cases of MLCT and *d–d** transitions [16]. Phosphorescence of Pt(IV) complexes could be assigned to the spin-forbidden intraligand optical transition of the platinized ptpy ligand due to the following reasons: the agreement between almost invariant position of the intraligand absorption band (314 ± 2 nm) of Pt(IV) complexes, invariant energy position of their phosphorescence spectra, and kinetics of its decay (λ_{max} 454 ± 1 nm, τ 320 ± 20 μs); the agreement between frequency of the vibrational progression [$(1.50 \pm 0.03) \times 10^3$ cm^{-1}] in the phosphorescence spectrum and the vibration frequency of C=C/C=N bonds of ptpy ligand. Indeed, the energy of singlet-triplet splitting $(10.1 \pm 0.1) \times 10^3$ cm^{-1} in Pt(IV) complexes agreed with the value expected for the intraligand optical transition.

Replacement of Pt(IV) with Rh(III) had practically no effect on position of the intraligand absorption band (~310 sh), whereas phosphorescence spectra underwent red shift shift of 500 ± 100 cm^{-1}, its decay time decreasing to 80–110 μs (Table 3). That reflected the mixed nature (IL/MLCT) of the lowest electron-excited state responsible for phosphorescence of Rh(III) complexes.

Despite almost invariant position of the intraligand absorption bands in the spectrum (~311 sh), phosphorescence of Ir(III) complexes was characterized by further red shift of $(1.6 \pm 0.2) \times 10^3$ cm^{-1} with respect to the Pt(IV) complexes as well as by further decrease of the phosphorescence decay time to 6 ± 1 μs. Hence, the MLCT contribution into the presumably intraligand spin-forbidden optical transition increased. The mixed nature of the (IL/MLCT) phosphorescence of Ir(III) complexes, opposed to the intraligand phosphorescence of Pt(IV) complexes, led to blue shift of the spectrum with decreasing the energy of d_π orbitals (complexes with σ-donor ethylendiamine ligand) and with decreasing the temperature by $(0.8 \pm 0.1) \times 10^3$ cm^{-1} (complexes with π-donor chelating ligands: dtc^-, OTf^-, and OAc^-) due to the more polar excited state.

To conclude, the energy positions of phosphorescence (457–514 nm) and long-wave absorption bands (340-485 nm) along with reduction (–1.5–3.0 V) and oxidations potential (0.45–1.25 V) of the cyclometallated complexes $[M(ptpy)_2(L\hat{}L)]^z$ could be purposefully changed by varying the metal nature [Ir(III), Rh(III), or Pt(IV)] and donor-acceptor properties of the chelating ligand (L^L).

EXPERIMENTAL

^1H and ^{19}F NMR spectra ($CDCl_3$ or DMSO-d_6) were recorded using the JNM-ECX400A spectrometer; IR spectra (KBr) were obtained with the IR Prestige-21 spectrometer belonging to the Collective Usage Center, Chemistry Department, Herzen Russian State Pedagogical University. Electronic absorption spectra

(CH_2Cl_2) were registered with the SF-2000 spectrophotometer. Phosphorescence spectra and kinetics of phosphorescence decay in CH_2Cl_2 and CH_3CN solutions (293 K) and in glassy (77 K) 1 : 1 2-methoxyethanol-ethanol mixture were recorded with the Flyuorat-02 Panorama spectrofluorimeter. Voltamperograms were recorded with the IPC-PRO instrument at 293 K in the cell with separated spaces of working (GC), auxiliary (Pt), and reference (Ag) electrodes in 0.1 mol/L $[N(C_4H_9)_4]PF_6$ solution in CH_3CN, $(CH_3)_2NCOH$, or in $C_6H_5CH_3$–CH_3CN 1 : 1. Peak potentials were given relative to the ferrocenium-ferrocene redox pair at potential scanning rate of 100 mV/s.

The complexes were prepared following the general procedure including the synthesis of $[Rh(ptpy)_2(\mu\text{-}Cl)]_2$, $[Ir(ptpy)_2(\mu\text{-}Cl)]_2$, and $[Pt(ptpy)_2Cl_2]$ [17, 18]; removal of AgCl precipitate by addition of two equivalents of acetonitrile solution of $AgNO_3$; addition of one equivalent of methanol solution of ethylenediamine or sodium salt of the chelating ligand L^L to the mixture. Solvent evaporation led to precipitation of the $[M(ptpy)_2(L\text{^}L)]$ [M = Rh(III), Ir(III); (L^L) = dtc^-, OAc^-, OTf^-] complexes, they were further purified by column chromatography (silica gel, dichloromethane as eluent). Yield 40–60%. Cationic complexes $[M(ptpy)_2EnPF_6$ [M = Rh(III), Ir(III)], $[Pt(ptpy)_2(L\text{^}L)]PF_6$ [(L^L) = dtc^-, OAc^-, OTf^-], and $[Pt(ptpy)_2En](PF_6)_2$ with yield of 40–60% were obtained by precipitation with KPF_6 saturated aqueous solution.

REFERENCES

1. Wong, W.-Y. and Ho, C.-L., *J. Mater. Chem*., 2009, vol. 19, no. 26, p. 4457. DOI: 10.1039/B819943D.
2. Xiao, L., Chen, Z., Qu, B., Luo, J., Kong, S., and Kido, J., *Adv. Funct. Mater*., 2011, vol. 23, no. 8, p. 926. DOI: 10.1002/adma. 201003128.
3. Ragni, R., Orselli, E., Kottas, G.S., Omar, G.H., Badudry, F., Pedoni, A., Naso, F., Forinola, G.M., and De Cola, M., *Eur. J. Chem*., 2009, vol. 15, no. 1, p. 136. DOI: 10.1002/chem. 200801270.
4. Guerchais, V. and Fillaut, J.-L., *Coord. Chem. Rev*., 2011, vol. 255, nos. 21–22, p. 2448. DOI: 10.1016/ ccr.2011.04.006.
5. Volpi, G., Garino, S., Salassa, L., Fiedler, J., Hardcastle, K.I., Gobetto, R., and Nervi C., *Eur. J. Chem*., 2009, vol. 15, no. 26, p. 6415. DOI: 10.1002/chem. 20081474.
6. Ma, D.-L., Wong, W.-L., Chung, W.-H., Chan, F.-Y., So, P.-K., Lai, T.-S., Zhou, Z.-Y., Leung, Y.-S., and Wong, K.-Y., *Angew. Chem. Int. Ed*., 2008, vol. 47, no. 20, p. 3735. DOI: 10.1002/anie.200705319.
7. Nakamoto, K., *Infrared and Raman Spectra of Inorganic and Coordination Compounds*, New York: John Wiley, 1986.
8. Kellner, R., Nikolov, G., and Trendafilova, N., *Inorg. Chim. Acta*., 1984, vol. 84, no. 2, p. 233. DOI: 10.1016/ S0020-1693 (00 82413-5.
9. DeArmond, K., Hanck, K.W., and Wertz, D.W., *Coord. Chem. Rev*., 1985, vol. 64, p. 65. DOI: 10.1016/0010-8545(85) 80042-4.
10. Mdleleni, M.M., Bridgewater, J.S., Watts, R.J., and Ford P.C., *Inorg. Chem*., 1995, vol. 34, no. 9, p. 2334. DOI: 10.1021/ic00113a013.
11. Koopmans, T., *Physics*, 1933, vol. 1, no. 1, p. 104.
12. Lever, A.B.P., *Inorganic Electronic Spectroscopy*, Amsterdam: Elsevier, 1984, 2nd ed.
13. Montalti, M., Credi, A., Prodi, L., and Gandolfi, T., *Handbook of Photochemistry*, Boca Raton CRS: Press/ Taylor Francis, 2006, p. 617.
14. Barigelletti, F., Sandrini, D., Maestri, M., V., and von Zelewsky, A., *Inorg. Chem*., 1988, vol. 27, no. 20, p. 3644. DOI: 10.1021/ic0293a041.
15. Colombo, M.G., Hauser, A., and Gudel, H.U., *Inorg. Chem*., 1993, vol. 32, no. 14, p. 3088. DOI: 10.1021/ ic00066a020.
16. Miskowski, M.M., Houlding, H.V., Che, C.-M., and Wang, Y., *Inorg. Chem*., 1993, vol. 32, no. 11, p. 2518. DOI: 10.1021/ic00063a052.
17. Brooks, J., Babayan, Y., Lamansky, S., and Thomson, M.E., *Inorg. Chem*., 2002, vol. 41, no. 12, p. 3055. DOI: 10.1021/ic0255508.
18. Kotlenok, E.A. and Balashev, K.P., *Russ. J. Gen. Chem*., 2013, vol. 83, no. 11, p. 2113. DOI: 10.1134/ S1070363213110273.